magnetochemistry

Article

Mechanical Detection of Magnetic Phase Transition in Suspended CrOCl Heterostructures

Xiaoxi Li [1,2,*,†], Xuanzhe Sha [1,2,†], Ning Yan [1,2] and Tongyao Zhang [1,2,*]

1 State Key Laboratory of Quantum Optics and Quantum Optics Devices, Institute of Opto-Electronics, Shanxi University, Taiyuan 030006, China
2 Collaborative Innovation Center of Extreme Optics, Shanxi University, Taiyuan 030006, China
* Correspondence: xiaoxili1987@sxu.edu.cn (X.L.); tongyao_zhang@sxu.edu.cn (T.Z.)
† These authors contributed equally to this work.

Abstract: With their outstanding mechanical and magnetic characteristics, two-dimensional magnetic materials have attracted wide attentions in the field of nanoelectromechanics and spintronics. By tuning the mechanical resonance with external knobs, such as strain, electric and magnetic control, nanoelectromechanical sensors with novel functionalities have been successfully demonstrated. Here, we investigate the mechanical properties of the suspended membranes with few-layered antiferromagnetic material CrOCl. The results show that the Young's modulus of CrOCl resonators is ~137.29 GPa by using a static detection method. Below the transition temperature T_N, the mechanical resonance is found to strongly depend on the magnetic fields with an enormous blueshift of ~3.1% in the magnetic-field-induced phase transition. In addition, we also found that the variation of strain of system $\Delta\epsilon$ was about 1.5×10^{-3} during the transition. Our study shows the great potential of two-dimensional magnetic materials in future nanoelectronic applications.

Keywords: nanomechanical resonators; Young's modulus; CrOCl; van der Waals heterostructures

Citation: Li, X.; Sha, X.; Yan, N.; Zhang, T. Mechanical Detection of Magnetic Phase Transition in Suspended CrOCl Heterostructures. *Magnetochemistry* **2022**, *8*, 170. https://doi.org/10.3390/magnetochemistry8120170

Academic Editor: Dinh Loc Duong

Received: 1 November 2022
Accepted: 23 November 2022
Published: 25 November 2022

1. Introduction

Since 2017, the family of two-dimensional magnetic materials (2DMMs) with intrinsic long-range magnetic order have been constantly expanding benefits from their prospects in spintronics. Among the numerous 2DMMs, such as CrI_3 [1], Fe_3GeTe_2 [2,3], $Cr_2Ge_2Te_6$ [4–6], V_5S_8 [7], in-plane rectangular structural magnets have increasingly attracted attention due to their air stability and large interfacial interactions [8–10]. As one kind, Chromium Oxychloride (CrOCl) [11–14] is an air-stable antiferromagnetic (AF) insulator, with a Neel temperature T_N of about 13.5 K, accompanied by a structural phase transition from the orthorhombic to monoclinic group. As temperature increases, a second magnetic phase transition in CrOCl is observed at 27 K [12], which exhibits similar phase transitions with the isostructural compound CrSBr [15]. Phase-transition behaviours with temperature and magnetic fields and spin-phonon coupling effects in the exfoliated CrOCl have been extensively reported [16–18]. Furthermore, a series of novel quantum physics are successively shown in other atomically thin van der Waals flakes interfaced with few-layered CrOCl, such as in-plane polarization in monolayer MoS_2 [19], interfacial-charge-coupled quantum Hall effect (QHE) in graphene and correlated insulator behaviours in Bernal-stacked bilayer graphene [20,21], indicating 2D CrOCl to be a fascinating platform for the investigation of exotic quantum electronic states.

Nanomechanical resonators based on 2DMMs offer an effective way to detect the phase transition and even control the magnetic states of the 2DMMs conversely. The mechanical resonance dependent on temperature, magnetic field, and strain has been investigated in many magnetic semiconductors and insulators over the past few years [22–27]. One recent example is that the spin-flip phase transition from AF to ferromagnetic (FM) phase in CrI_3 was found to be driven by the magnetostriction effect [22]. In addition, the Young's modulus and magnetic properties of a $Cr_2Ge_2Te_6$ system were studied in detail [27]. Furthermore, we established a suspended CrOCl/graphene vdW nanomechanical resonator recently and demonstrated the electric and magnetic field tuning of mechanical resonance [23]. However, the mechanical properties, such as Young's modulus, as well as their changes during phase transitions, of few-layered CrOCl flakes are still unclear.

In this work, the CrOCl/graphene heterostructure suspended on drummed holed h-BN (~300 nm) was fabricated using the dry-transfer method. We first studied the Young's modulus of the CrOCl resonators (~137.29 GPa) with the nano-indention method using an Atomic Force Microscope (AFM). At temperatures below the Néel temperature of CrOCl, an enormous blueshift of ~3.1% of the mechanical resonant frequency appears by tuning the magnetic fields. Moreover, the variation of strain of system $\Delta\epsilon$ ~1.5×10^{-3} is evaluated, confirming that the blueshift of resonant frequency is caused by the shrink of CrOCl membrane along with the magnetostriction effect.

2. Materials and Fabrications

In this paper, atomically thin flakes of graphene (Gr), CrOCl, h-BN were directly mechanically exfoliated onto a SiO_2/Si substrate from the high-quality single crystal. CrOCl/graphene heterostructures are fabricated in ambient conditions using the dry-transfer method [28]. For extracting the elastic properties, circular drum-like structures with radius R = 1.5 µm were patterned in the support layer h-BN (~300 nm in thickness) by reactive ion etching (RIE). Drummed h-BN was transferred onto the surface of Au/Ti (30/15 nm) electrostatic modulating electrode using PPC (Propylene–Carbonate), then the CrOCl/Gr heterostructures were deposited onto the drummed h-BN/Au. The final stacks on SiO_2/Si substrates were annealed at 400 °C for 60 min in a high-vacuum environment to completely remove the residual polymer. Metal electrodes (Ti/Au = 5/250 nm) were fabricated by standard electron beam lithography (EBL) using a Zeiss Sigma 300 SEM with a Raith Elphy Quantum graphic writer, RIE and electron beam evaporation (EBV). The schematics cross-section of the final drumhead CrOCl resonators can be seen in Figure 1a. As shown in Figure 1b, typical CrOCl/graphene heterostructures were suspended on the surface of a drummed h-BN array well to form a series of free-standing nano-resonators. The SEM image of CrOCl resonators (Figure 1c) captured from Zeiss Sigma 300 SEM further confirms that no collapse or wrinkles occurred in the device.

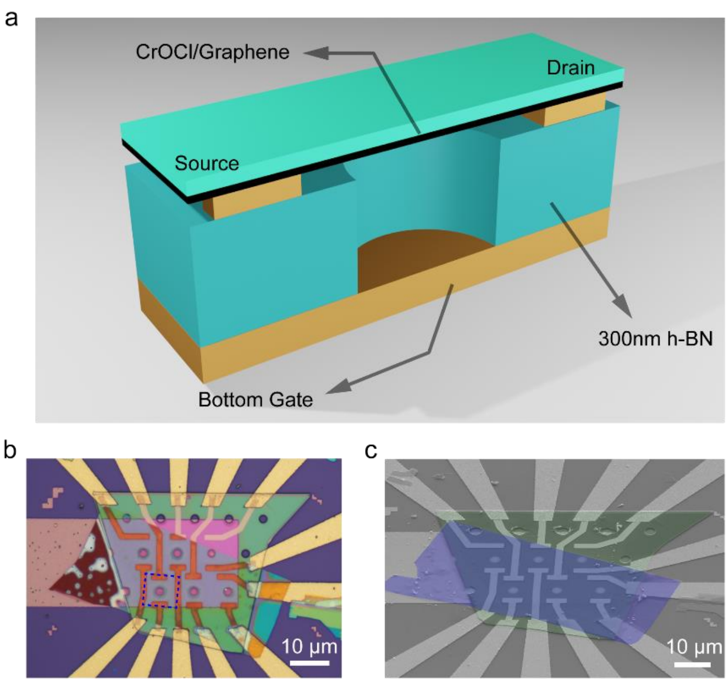

Figure 1. The suspended CrOCl/graphene heterostructure resonators. (**a**) Schematic diagram of the

fabricated CrOCl drum resonators (cross-section view). (**b**) Optical image of CrOCl resonators. (**c**) SEM image of the device in (**b**), which confirms that the CrOCl/graphene drums are suspended well. Suspended CrOCl/graphene heterostructure and holed h-BN were marked in purple and green boxes, respectively.

3. Results and Discussion

After the device fabrication, we then characterized the deflection response of the CrOCl resonators with a Bruker Dimension Icon AFM using the force nano-indention method with the probe of TESPA-V2. Before nano-indenting, we confirmed the location of suspension of the drumhead resonator using AFM Tapping mode, as seen in the white solid circle in Figure 2a. Then, the tip of the AFM cantilever was positioned in the center of the drummed hole to induce out-of-plane deflection (Figure 2b), and a typical force-deflection curve can be detected using the nano-indention method after alignment, as shown in Figure 2c.

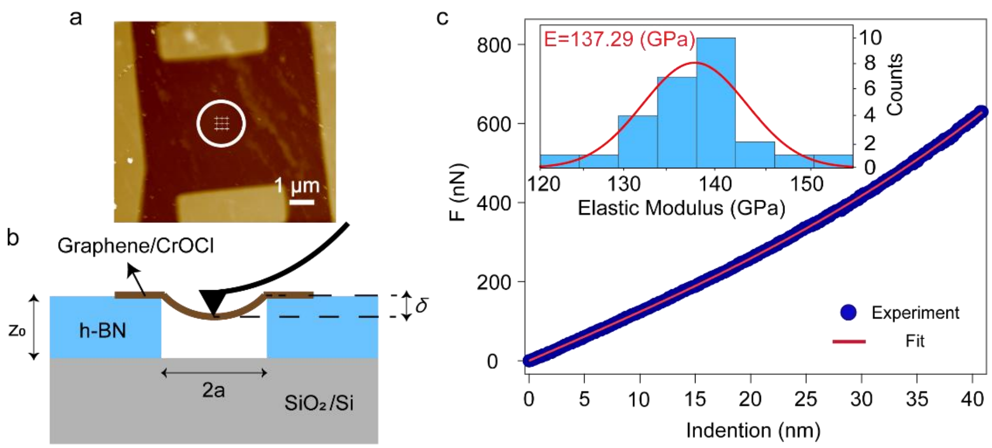

Figure 2. Young's modulus of the CrOCl resonators. (**a**) Morphology image of a typical CrOCl resonator of dashed blue-boxed area in Figure 1b. Suspended area is depicted by the white solid circle, and the white crosshair represents the position that we applied nano-indention measurement. (**b**) Schematic diagram of force detection of CrOCl resonators. (**c**) Typical force versus indention curve of our device. The inset shows a histogram of the Young's modulus extracted from 27 points in (**a**). The solid line is a normal fit of the histogram.

For a suspended, circular, linear elastic membrane under a central load, ignoring the effect of tip radius and the adhesive force between the AFM tip and sample, the force we applied on the surface of CrOCl resonators can be simplified as [29–31]:

$$F = \pi\sigma_0 h\delta + \frac{Eh}{q^3a^2}\delta^3, \quad (1)$$

where F is the applied force, σ_0 is the pre-stress in the suspended CrOCl, δ is the deformation depth, h is the effective thickness of the suspended CrOCl/graphene (taken as 30 nm), E is the Young's modulus of sample, $q = 1/\left(1.05 - 0.15\nu - 0.16\nu^2\right)$, where ν is Poisson's ratio and set to 0.3 as an estimation, and a = 1.5 μm is the radius of the holed h-BN. Therefore, the Young's modulus of CrOCl resonators can be calculated based on Equation (1). 9 points around the center in each hole (white crosshair in Figure 2a) are chosen every time and three holes have been tested to improve the data reliability, the histogram statistics is shown in the inset of Figure 2c. The Young's modulus of the sample was about 137.29 GPa, revealed by a normal fit of the histogram.

We investigated the mechanical resonance of the CrOCl resonators in a cryostat (AttoDRY 1000) under a vacuum below 10^{-2} mbar. A DC static voltage (V_g = −20~20 V) and

AC perturbation voltage (lower than ~4 mV) were combined by a bias tee to supply between the graphene and Au gate, and the eigenfrequency of the CrOCl/graphene heterostructure was detected using optical interferometric detection. In our experiments, a beam of the input laser (λ = 655 nm) with controllable power density (~10 μWμm^{-2}) was focused on the sample with a spot radius of ~1.5 μm, while the reflected laser was detected by using a fast photoreceiver. The out-of-plane displacement as a function of driven frequency was measured by a vector network analyzer.

At the base temperature of 5 K, the mechanical resonance of a CrOCl resonator is shown in Figure 3a, with the perpendicular magnetic field sweeping from 3 T to 4.7 T at a DC static voltage V_g = 10 V. The resonant frequency of CrOCl resonator f_0 was around ~63.7 MHz under low magnetic field. When magnetic field B reached ~3.7 T to 4.1 T, a quite large blueshift of ~3.1% was observed, which is significantly higher than other reported AF resonator systems [22]. For comparison, we reverse-scanned the magnetic field from 4.7 T to 3 T and recorded the dependence of actuation frequency f on vibration amplitude (Figure 3b). The resonance data in Figure 3a,b can be fitted by a Lorentzian model, with the resonant frequency f_0 versus magnetic field plotted in Figure 3c. A hysteresis type of f_0 is clearly observed when the magnetic field is scanned back and forth, being consistent with the magnetic phase transition of bulk CrOCl reported in earlier works [17] and of ultra-thin CrOCl layer in our recent publication [23].

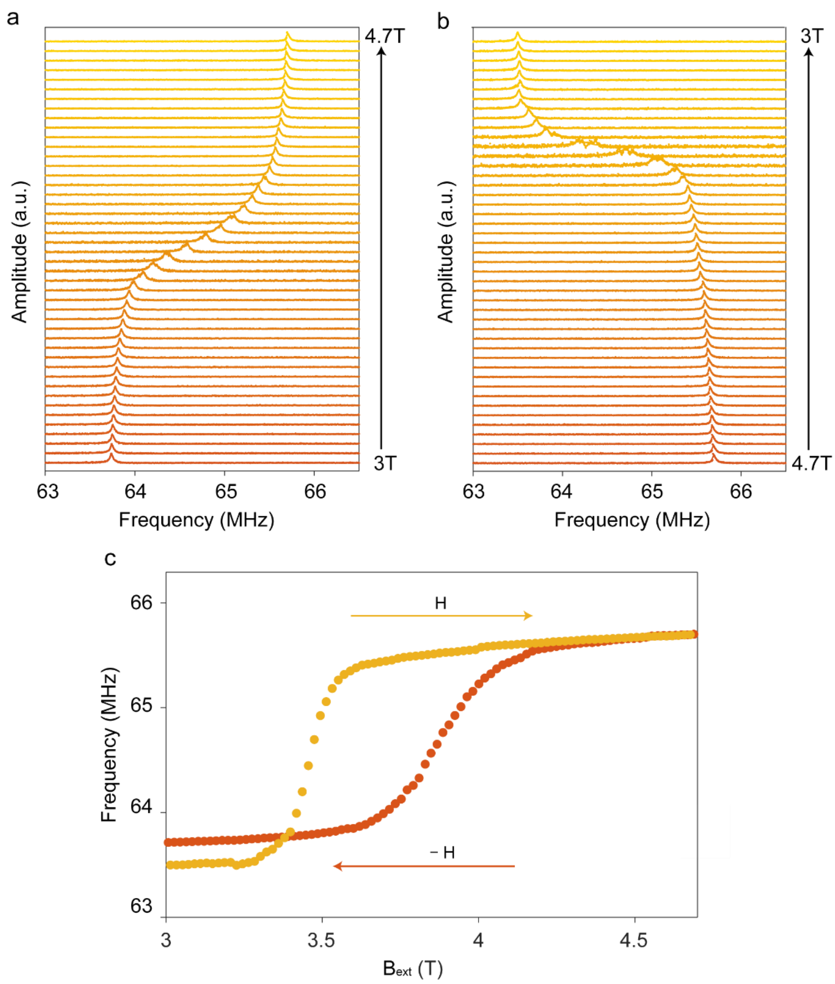

Figure 3. Mechanical resonance of the CrOCl resonators versus perpendicular magnetic field. (**a**) Mechanical resonance curves with the external magnetic field sweeping from 3 T to 4.7 T, and a reversed scan from 4.7 T to 3 T shown in (**b**). (**c**) Resonant frequency f_0 of CrOCl resonators as a function of perpendicular magnetic field revealed from the fittings of (**a**,**b**). The curves with yellow and red color represent forward and reverse sweeping respectively.

The obvious blueshift of mechanical resonance we observed may result from the strain change during the magnetic phase transition because of the magnetostriction effect. Therefore, we focused on the strain-tuning performance of the CrOCl resonators. Figure 4a illustrates the colour map of resonant frequency f_0 versus DC static gate voltage V_g at various magnetic fields B, ranging from 3 T to 4.7 T at the temperature of 5 K. A noticeable step of resonant frequency in the blue and red region can further demonstrate the change of resonant frequency. For the circular drum-like structures in our CrOCl resonators, the initial strain ϵ can be estimated using the equation as follows [32,33]:

$$4\pi f_0^2 = 4.92 Y_{eff} \epsilon m_{eff}^{-1} - 0.271 \varepsilon_0 \pi R^2 V_g^2 \left(m_{eff} z_0^3 \right)^{-1} \tag{2}$$

where $Y_{eff} = E \cdot h$ ~137.29 × 30 = 4.1 × 10^4 N/m is the effective 2D Young's modulus according to the AFM measurement, R = 1.5 μm is the radius of the drum, z_0 = ~300 nm is the distance from Au gate to the CrOCl/graphene heterostructure, m_{eff} is the effective mass of CrOCl/graphene heterostructure, and h is the thickness of the suspended membrane. Here, we suppose the Young's modulus of our studied system is still reliable at cryogenic temperatures, which is reasonable as suggested by theoretical calculations [34]. The linear relation between ${f_0}^2$ and ${V_g}^2$ with different magnetic fields extracted from Figure 4a is plotted in Figure 4b. Therefore, according to Equation (2), initial strain ϵ, as the intercept of curves, can be calculated readily. As shown in Figure 4c, there is an obvious strain change ($\Delta\epsilon$ ~1.5 × 10^{-3}) at the point of phase transition in CrOCl resonators during the process of sweeping the magnetic fields. This indicates that the blueshift of the resonate frequency in our devices is caused by the enlargement of built-in strain of the magnetostriction effect.

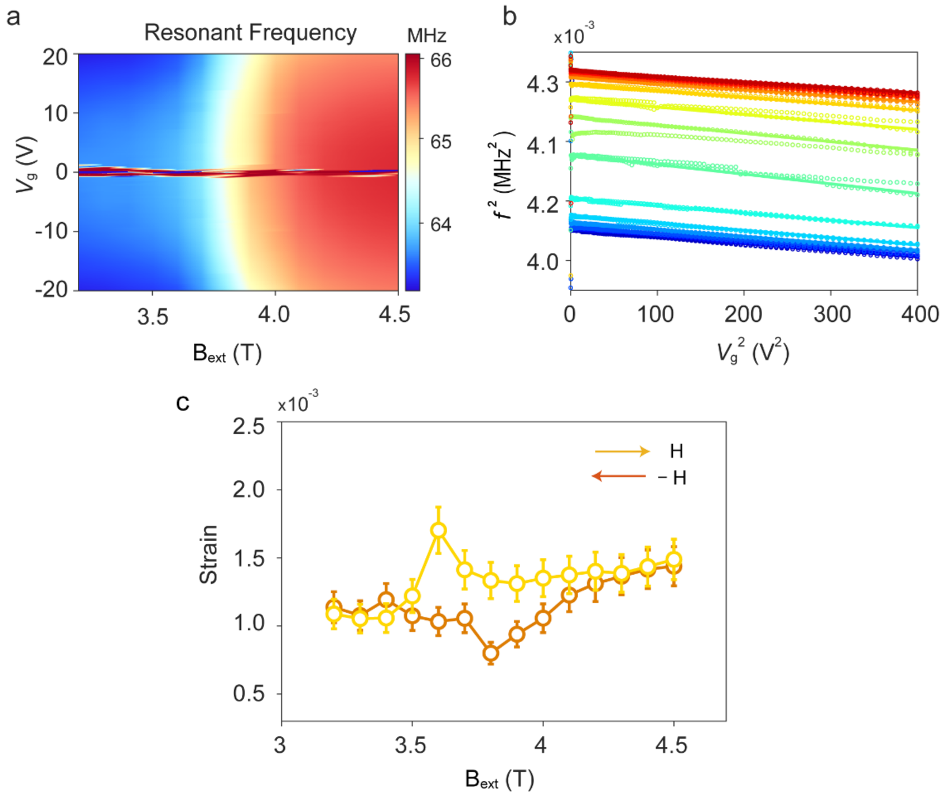

Figure 4. Strain-tuning of the phase transition in CrOCl resonators. (**a**) Colour map of the resonant frequency as a function of gate voltage V_g and magnetic fields for CrOCl resonators at a temperature of 5 K. (**b**) Linear relation between ${f_0}^2$ and ${V_g}^2$ with various magnetic fields sweeping from 3 T to 4.7 T. The solid line is a linear fit of data (dots). The curves from blue to red color represent different magnetic fields from 3.2 T to 4.5 T. (**c**) The stain hysteresis of CrOCl resonators versus magnetic fields. The curves with yellow and red color represent forward and reverse sweeping respectively.

It is worth noting that the value of Young's modulus is measured in a CrOCl/graphene sample, so the contribution of graphene may dominate the Young's modulus of the heterostructure. However, in such an AF/graphene type heterostructure, graphene itself does not devote to the magnetoelastic process which is related to a perpendicular magnetic field. Additionally, the geometry of the drum-like graphene prevents the local interferometry detection from sensing the chemical-oscillation-induced mechanical resonance shift in the quantum Hall regime. Therefore, the remarkable resonance frequency shift mainly stems from the magnetic phase transition of the ultrathin CrOCl layer. From the mechanical hysteresis loop uncovered from resonant frequency and strain in Figures 3c and 4c, only one transition process can be found when increasing the magnetic field, which is different from the two distinct transitions discovered by magnetic moment measurement or tunnelling magnetoresistance. From a macroscopic view, the probe of mechanical resonance directly relates to the effective elastic coefficient and the effective mass of the resonator. Hence, resonance detection may be insensitive to the phase transitions and weakly related to thermal expansion coefficient and compressibility coefficient. The spin-flop transition of the CrOCl membrane thus may not be efficiently separated from magnetic state transition by the resonance probe.

4. Conclusions

Fabricating suspended few-layered CrOCl resonators offers more opportunities to explore the mechanical properties of CrOCl flakes. The nanoindentation technique gives the value of Young's modulus of CrOCl/graphene heterostructures of about 137.29 GPa, which provides an exact data support for the calculation of strain during phase transition below T_N. Mechanical resonance was successfully measured and shows an enormous blueshift with the variation of magnetic fields. In addition, we also found that the strain change is ~1.5×10^{-3} through calculation in the magnetic phase transition of CrOCl. Our study offers an experimental foundation for the potential applications of two-dimensional magnetic materials on ultra-sensitive detection and micro-nano sensors.

Author Contributions: Conceptualization, methodology, formal analysis, writing—original draft preparation, X.L. and T.Z.; sample fabrication, data curation, discussion, X.L., X.S., N.Y. and T.Z. All authors have read and agreed to the published version of the manuscript.

Funding: This research was funded by the National Natural Science Foundation of China (NSFC) (Grant Nos. U21A6004, 12004389, 62274180, 12204287).

Institutional Review Board Statement: Not applicable.

Informed Consent Statement: Not applicable.

Data Availability Statement: Data is available from the corresponding author on reasonable request.

Acknowledgments: The authors appreciate the help of Zheng Han in the valuable revision suggestions of this work.

Conflicts of Interest: The authors declare no conflict of interest.

References

1. Huang, B.; Clark, G.; Navarro-Moratalla, E.; Klein, D.R.; Cheng, R.; Seyler, K.L.; Zhong, D.; Schmidgall, E.; McGuire, M.A.; Cobden, D.H.; et al. Layer-dependent ferromagnetism in a van der Waals crystal down to the monolayer limit. *Nature* **2017**, *546*, 270–273. [CrossRef] [PubMed]
2. Deng, Y.; Yu, Y.; Song, Y.; Zhang, J.; Wang, N.Z.; Sun, Z.; Yi, Y.; Wu, Y.Z.; Wu, S.; Zhu, J.; et al. Gate-tunable room-temperature ferromagnetism in two-dimensional Fe_3GeTe_2. *Nature* **2018**, *563*, 94–99. [CrossRef] [PubMed]
3. Wang, X.; Tang, J.; Xia, X.; He, C.; Zhang, J.; Liu, Y.; Wan, C.; Fang, C.; Guo, C.; Yang, W.; et al. Current-driven magnetization switching in a van der Waals ferromagnet Fe_3GeTe_2. *Sci. Adv.* **2019**, *5*, eaaw8904. [CrossRef]
4. Gong, C.; Li, L.; Li, Z.; Ji, H.; Stern, A.; Xia, Y.; Cao, T.; Bao, W.; Wang, C.; Wang, Y.; et al. Discovery of intrinsic ferromagnetism in two-dimensional van der Waals crystals. *Nature* **2017**, *546*, 265–269. [CrossRef] [PubMed]

5. Wang, Z.; Zhang, T.; Ding, M.; Dong, B.; Li, Y.; Chen, M.; Li, X.; Huang, J.; Wang, H.; Zhao, X.; et al. Electric-field control of magnetism in a few-layered van der Waals ferromagnetic semiconductor. *Nat. Nanotechnol.* **2018**, *13*, 554–559. [CrossRef] [PubMed]
6. Li, X.; Dong, B.; Sun, X.; Wang, H.; Yang, T.; Yu, G.; Han, Z.V. Perspectives on exfoliated two-dimensional spintronics. *J. Semicond.* **2019**, *40*, 081508. [CrossRef]
7. Niu, J.; Yan, B.; Ji, Q.; Liu, Z.; Li, M.; Gao, P.; Zhang, Y.; Yu, D.; Wu, X. Anomalous Hall effect and magnetic orderings in nanothick V_5S_8. *Phys. Rev. B* **2017**, *96*, 075402. [CrossRef]
8. Gong, C.; Zhang, X. Two-dimensional magnetic crystals and emergent heterostructure devices. *Science* **2019**, *363*, 706. [CrossRef] [PubMed]
9. Song, T.; Sun, Q.; Anderson, E.; Wang, C.; Qian, J.; Taniguchi, T.; Watanabe, K.; McGuire, M.A.; Stöhr, R.; Xiao, D.; et al. Direct visualization of magnetic domains and moiré magnetism in twisted 2D magnets. *Science* **2021**, *374*, 1140–1144. [CrossRef]
10. Telford, E.J.; Dismukes, A.H.; Lee, K.; Cheng, M.; Wieteska, A.; Bartholomew, A.K.; Chen, Y.; Xu, X.; Pasupathy, A.N.; Zhu, X.; et al. Layered Antiferromagnetism Induces Large Negative Magnetoresistance in the van Der Waals Semiconductor CrSBr. *Adv. Mater.* **2020**, *32*, 2003240. [CrossRef] [PubMed]
11. Christensen, A.; Johansson, N.T.; Quezel, S. Preparation and Magnetic Properties of CrOCl. *Acta Chem. Scand. A* **1975**, *28*, 1171–1174. [CrossRef]
12. Angelkort, J.; Wölfel, A.; Schönleber, A.; van Smaalen, S. Observation of strong magnetoelastic coupling in a first-order phase transition of CrOCl. *Phys. Rev. B* **2019**, *80*, 144416. [CrossRef]
13. Miao, N.; Xu, B.; Zhu, L.; Zhou, J.; Sun, Z. 2D Intrinsic Ferromagnets from van der Waals Antiferromagnets. *J. Am. Chem. Soc.* **2018**, *140*, 2417–2420. [CrossRef]
14. Bykov, M.; Bykova, E.; Dubrovinsky, L.; Hanfland, M.; Liermann, H.; van Smaalen, S. Pressure-induced normal-incommensurate and incommensurate- commensurate phase transitions in CrOCl. *Sci. Rep.* **2015**, *5*, 9647. [CrossRef] [PubMed]
15. Liu, W.; Guo, X.; Schwartz, J.; Xie, H.; Dhale, N.U.; Sung, S.H.; Kondusamy, A.L.N.; Wang, X.; Zhao, H.; Berman, D.; et al. A three-stage magnetic phase transition revealed in ultrahigh-quality van der Waals bulk magnet CrSBr. *ACS Nano* **2022**, *16*, 15917–15926. [CrossRef]
16. Zhang, T.; Wang, Y.; Li, H.; Zhong, F.; Shi, J.; Wu, M.; Sun, Z.; Shen, W.; Wei, B.; Hu, W.; et al. Magnetism and Optical Anisotropy in van der Waals Antiferromagnetic Insulator CrOCl. *ACS Nano* **2019**, *13*, 11353–11362. [CrossRef]
17. Gu, P.; Sun, Y.; Wang, C.; Peng, Y.; Zhu, Y.; Cheng, X.; Yuan, K.; Lyu, C.; Liu, X.; Tan, Q.; et al. Magnetic Phase Transitions and Magnetoelastic Coupling in a Two-Dimensional Stripy Antiferromagnet. *Nano Lett.* **2022**, *22*, 1233–1241. [CrossRef] [PubMed]
18. Qing, X.; Li, H.; Zhong, C.; Zhou, P.; Dong, Z.; Liu, J. Magnetism and spin exchange coupling in strained monolayer CrOCl. *Phys. Chem. Chem. Phys.* **2020**, *22*, 17255–17262. [CrossRef] [PubMed]
19. Zheng, X.; Wei, Y.; Zhang, X.; Wei, Z.; Luo, W.; Guo, X.; Liu, J.; Peng, G.; Cai, W.; Huang, H.; et al. Symmetry Engineering Induced In-Plane Polarization in MoS_2 through Van der Waals Interlayer Coupling. *Adv. Funct. Mater.* **2022**, *32*, 2202658. [CrossRef]
20. Wang, Y.; Gao, X.; Yang, K.; Gu, P.; Dong, B.; Jiang, Y.; Watanabe, K.; Taniguchi, T.; Kang, J.; Lou, W.; et al. Flavoured quantum Hall phase in graphene/CrOCl heterostructures. *Nat. Nanotechnol.* **2022**. [CrossRef]
21. Yang, K.; Gao, X.; Wang, Y.; Zhang, T.; Gu, P.; Luo, Z.; Zheng, R.; Cao, S.; Wang, H.; Sun, X.; et al. Realization of graphene logics in an exciton-enhanced insulating phase. *arXiv* **2021**. [CrossRef]
22. Jiang, S.; Xie, H.; Shan, J.; Mak, K.F. Exchange magnetostriction in two-dimensional antiferromagnets. *Nat. Mater.* **2022**, *19*, 1295–1299. [CrossRef] [PubMed]
23. Zhang, T.; Wang, H.; Xia, X.; Yan, N.; Sha, X.; Huang, J.; Watanabe, K.; Taniguchi, T.; Zhu, M.; Wang, L.; et al. A monolithically sculpted van der Waals nano-opto-electro-mechanical coupler. *Light Sci. Appl.* **2022**, *11*, 48. [CrossRef] [PubMed]
24. Šiškins, M.; Lee, M.; Mañas-Valero, S.; Coronado, E.; Blanter, Y.M.; van der Zant, H.S.J.; Steeneken, P.G. Magnetic and electronic phase transitions probed by nanomechanical resonators. *Nat. Commun.* **2020**, *11*, 2698. [CrossRef] [PubMed]
25. Šiškins, M.; Sokolovskaya, E.; Lee, M.; Mañas-Valero, S.; Davidovikj, D.; van der Zant, H.S.J.; Steeneken, P.G. Tunable strong coupling of mechanical resonance between spatially separated $FePS_3$ nanodrums. *Nano Lett.* **2022**, *22*, 36–42. [CrossRef]
26. Lee, M.; Šiškins, M.; Mañas-Valero, S.; Coronado, E.; Steeneken, P.G.; van der Zant, H.S.J. Study of charge density waves in suspended 2H-TaS_2 and 2H-$TaSe_2$ by nanomechanical resonance. *Appl. Phys. Lett.* **2021**, *118*, 193105. [CrossRef]
27. Šiškins, M.; Kurdi, S.; Lee, M.; Slotboom, B.J.M.; Xing, W.; Mañas-Valero, S.; Coronado, E.; Jia, S.; Han, W.; van der Sar, T.; et al. Nanomechanical probing and strain tuning of the Curie temperature in suspended $Cr_2Ge_2Te_6$ heterostructures. *npj 2D Mater. Appl.* **2022**, *6*, 41. [CrossRef]
28. Castellanos-Gomez, A.; Buscema, M.; Molenaar, R.; Singh, V.; Janssen, L.; van der Zant, H.S.J.; Steele, G.A. Deterministic transfer of two-dimensional materials by all-dry viscoelastic stamping. *2D Mater.* **2014**, *1*, 011002. [CrossRef]
29. Lee, C.; Wei, X.; Kysar, J.W.; Hone, J. Measurement of the elastic properties and intrinsic strength of monolayer graphene. *Science* **2008**, *321*, 385–388. [CrossRef] [PubMed]
30. Soler-Crespo, R.A.; Mao, L.; Wen, J.; Nguyen, H.T.; Zhang, X.; Wei, X.; Huang, J.; Nguyen, S.T.; Espinosa, H.D. Atomically thin polymer layer enhances toughness of graphene oxide monolayers. *Matter* **2019**, *1*, 369–388. [CrossRef]
31. Wei, X.; Mao, L.; Soler-Crespo, R.A.; Paci, J.T.; Huang, J.; Nguyen, S.T.; Espinosa, H.D. Plasticity and ductility in graphene oxide through a mechanochemically induced damage tolerance mechanism. *Nat. Commun.* **2015**, *6*, 8029. [CrossRef] [PubMed]

32. Sazonova, V.S. A Tunable Carbon Nanotube Resonator. Ph.D. Thesis, Cornell University, Ithaca, NY, USA, 2006.
33. Chen, C. Graphene NanoElectroMechanical Resonators and Oscillators. Ph.D. Thesis, Cornell University, Ithaca, NY, USA, 2013.
34. Jiang, J.; Wang, J.; Li, B. Young's modulus of graphene: A molecular dynamics study. *Phys. Rev. B* **2009**, *80*, 113405. [CrossRef]